Lunar Surface Magnetometer

PALMER DYAL, CURTIS W. PARKIN, AND CHARLES P. SONETT

Abstract—The lunar surface magnetometer is one of five instruments in the Apollo lunar surface experiments package (ALSEP). It measures three components of the vector magnetic field in the range 0 to 400γ with a resolution of 0.2γ and a frequency response from dc to 3 Hz. This instrument also has a gradient measuring capability, making it an automatic magnetic observatory on the lunar surface. The magnetometer experiment deployed by Astronauts Conrad and Bean on Apollo 12 has measured a steady magnetic field of approximately 36γ on the lunar surface. During each lunar day–night period the magnetic fields in the geomagnetic tail, transition zone, and interplanetary region are superimposed upon this steady field. Measurements of the induced lunar magnetic field will permit the interior electrical conductivity and temperature to be calculated.

Introduction

ELECTROMAGNETIC properties of a planetary body can yield valuable information concerning its present physical state and evolutionary history. Earth and satellite magnetic-field measurements have proved to be useful tools for determining the electromagnetic properties of the earth's interior and its solar-wind and ionospheric environments.

An extension of these magnetic-field measurement techniques has been used on the Apollo 12 mission to investigate the electromagnetic properties of the moon. The magnetometer is located in the Ocean of Storms, a mare-type sea of smooth uniform surface features that make the site ideal for first measurements of whole-moon fields. Large mountains or craters would be more likely to possess local electromagnetic inhomogeneities, which would have hindered making whole-body lunar-field measurements with a single instrument.

Magnetometer measurements are used to determine the lunar response to fluctuations in the interplanetary magnetic field and to measure the time-invariant field associated with the whole moon and with local sources. Measurements of the induced lunar magnetic field permit the electrical conductivity of the lunar interior to be calculated. Because electrical conductivity is a function of temperature, these magnetic-field measurements provide information on the thermal state of the lunar interior. Such information on the interior temperature of the moon is crucial for differentiation between existing theories of lunar formation and history.

The fluxgate magnetometer (shown in Fig. 1) measures three vector components of the magnetic field as a function of time on the lunar surface. This magnetometer is small, lightweight, and has sufficient dynamic range to be integrated with the Apollo lunar surface experiment package (ALSEP) deployed by astronauts during their exploration of the moon. This paper describes the magnetometer instrument used to measure the magnetic field at the Apollo 12 landing site.

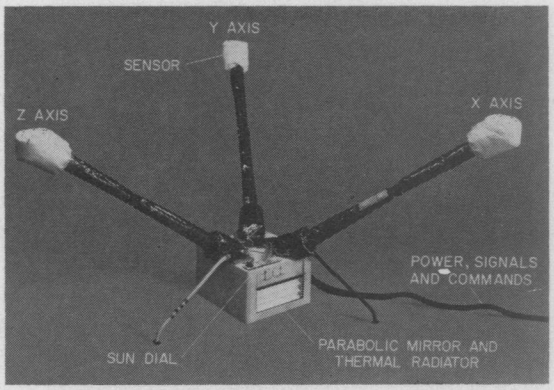

Fig. 1. Lunar surface magnetometer as deployed on the moon. The sensors are at the top end of the booms and approximately 70 cm above the lunar surface. The electronics and motor drive assembly are located in the box, encased in a thermal blanket. Heat rejection during lunar day and retention during lunar night are controlled by a parabolic reflector array on two sides of the electronics box. The astronaut bubble level and azimuthal shadowgraph are shown on top of the box. Power, digital signals, and commands are provided through the ribbon cable which connects to the ALSEP central-station telemetry receiver and transmitter.

Background and Theory of the Experiment

The purpose of the magnetometer experiment is to measure the magnetic field on the lunar surface and to determine from these measurements some of the deep-interior electrical properties of the moon. This experiment will also help to elucidate the interaction between the solar plasma and the lunar surface.

Recent measurements obtained before the Apollo 12 landing made considerable progress in the determination of the electrodynamic properties of the moon. Magnetic-field measurements from lunar orbital satellites such as Luna 10 [1] and Explorer 35 [2], [3] indicated an upper limit of 8 γ for the global surface field and indicated a remanent or permanent magnetic dipole moment for the whole moon of less than 10^{20} G·cm^3. Thus the lunar dipole moment should be less than 10^{-5} that of the earth. The remanent magnetization for surface material has been measured using some of the Apollo 11 samples, and the results indicate a range from 10^{-5} to 10^{-2} EMU/g [4].

The relative permeability μ of the lunar surface material can be estimated from the magnet experiment results of deWys [5] from Surveyors V and VI. deWys re-

Manuscript received May 18, 1970. This paper was presented at the 1970 IEEE International Geoscience Electronics Symposium, Washington, D. C., April 14–17.

The authors are with NASA, Ames Research Center, Moffett Field, Calif.

ported the presence of less than 1 percent by volume of magnetic iron material. By assuming this material to be magnetite and by using the dependence of permeability upon the magnetite content of rocks as given by Keller and Frischnecht [6], a relative permeability μ of 1.04 is derived for lunar surface material. Behannon [7] placed an upper limit of 1.8 on the bulk relative permeability by studying the Explorer 35 magnetometer measurements as the moon traversed the neutral sheet in the geomagnetic tail.

The relative dielectric constant ϵ of the surface material has been measured by earth- and satellite-based radar experiments. Hagfors [8], in his review of earth-based observations of the moon, showed a relative dielectric constant of 2.6 to be consistent with backscattered measurements at 10^8 Hz. Brown *et al.* [9] estimated a value for ϵ of 3.5 ± 0.7 at 10^{10} Hz by using data from the radar altimeter and the Doppler velocity sensor of the Surveyor III spacecraft.

The conductivity σ of the lunar surface material has been calculated by Kopal [10] from radiometer and radar data to be $\approx 10^{-4}$ mho/m at 3×10^8 Hz. More recently, Strangway [11] estimated the surface dc conductivity to be 10^{-13} to 10^{-16} mho/m, based upon investigations of radar scattering from the lunar surface. Explorer 35 magnetometer measurements by Colburn *et al.* [12] indicate a maximum whole-body conductivity of 10^{-6} mho/m for a homogeneous moon.

Analysis of the time-series magnetic-field measurements on the lunar surface can be conveniently divided into two parts. The first part covers field fluctuations with periods longer than 10 days, and the second part covers higher frequency phenomena with periods between 10 days and 1 second. The long-period measurements are associated either with remanent sources localized near the landing site or with the entire moon. The magnetic field measured on the lunar surface is the vector sum of the lunar, terrestrial, and solar magnetic fields. The selenomagnetic field associated with the whole moon or with a localized portion of the moon should have small amplitude variations for time periods less than 10 days and can, therefore, be separated from the high-frequency fluctuations by measurements obtained through one complete revolution of the moon around the earth. Simultaneous measurements from the Apollo 12 magnetometer and the Explorer 35 magnetometer (in lunar orbit) permit calculation of the size, location in the moon, and magnetic moment of the source. The orbiting magnetometer has a periselene of 1.48 lunar radii (R_m), an aposelene of 5.4 R_m, and an orbital period of approximately 11.5 hours [2].

The short-period measurements involve transient induction of fields in the moon by the solar field and by the earth's field at different locations in the orbit of the moon. The properties of the driving medium, that is, of the solar plasma or the earth's field, must also be considered in detail in order for one to understand the steady-state and transient magnetic fields on the lunar surface. The solar plasma or solar wind emanates from the solar atmosphere and passes the moon at a velocity of approximately 400 km/s. The high electrical conductivity of the solar wind allows the magnetic fields to be "frozen in" and carried along at the characteristic speed of the plasma. Such fields, which have been measured as a regular feature of the solar wind, originate with the plasma in the atmosphere of the sun. Because of the rotation of the sun, the solar magnetic field spirals out from the solar atmosphere in a pattern that makes an angle of approximately 45° with the direction of solar-wind flow near the orbit of the earth. The magnitude of the solar field near the earth is normally about 5 γ, and the density of the plasma is approximately 5 particles/cm^3. The moon also passes through the heated solar-wind plasma in the magnetosheath between the bow shock and the geomagnetic tail. Typical magnetic field amplitudes in the magnetosheath and geomagnetic tail at the lunar orbit are 7 and 9 γ, respectively.

The interplanetary magnetic field carries waves of various types which are associated with the different plasma modes in the solar wind [13]. These hydromagnetic waves intercept and electromagnetically excite the moon in a manner similar to magnetotelluric excitation on earth. McDonald [14] has applied this method to the earth by using the secular variations in the geomagnetic field to determine the electrical conductivity of the earth mantle.

Gold [15], in his analysis of the interaction of the moon with the solar wind, assumed that the electrodynamic interaction could be characterized by a Cowling time constant. Gold postulated that the time constant would be long compared to the rotation period and that a magnetosphere and accompanying shock wave would be produced. Magnetometers on Explorer 35 [2], [3] did not detect a bow shock.

Colburn *et al.* [12] and Sonett [16] extended this analysis to include the case in which a steady-state current is generated in the moon and closes in the solar plasma. An electric field

$$\boldsymbol{E} = \boldsymbol{V} \times \boldsymbol{B} \tag{1}$$

is produced as the solar magnetic field $\boldsymbol{B}$, frozen in the solar plasma, sweeps by the moon with a relative velocity $\boldsymbol{V}$. The current driven by this electric field will cause distortion of the magnetic field as it diffuses into the lunar interior. The current system induces a toroidal magnetic field with a magnitude inversely proportional to the total resistence to current flow through the moon [see Fig. 2(a)].

This toroidal model was used by Colburn *et al.* [12] in analysis of the Explorer 35 magnetic-field measurements to determine an effective bulk electrical conductivity of 10^{-6} mho/m for the whole moon. By similar analysis of Explorer 35 magnetic-field measurement, Ness [17] found the upper limit of the conductivity to be 10^{-5} mho/m. Colburn *et al.* and Ness assumed displacement currents to be negligible, the driving mag-

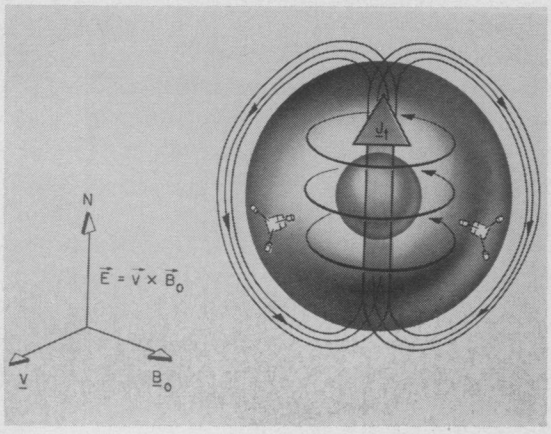

(a)

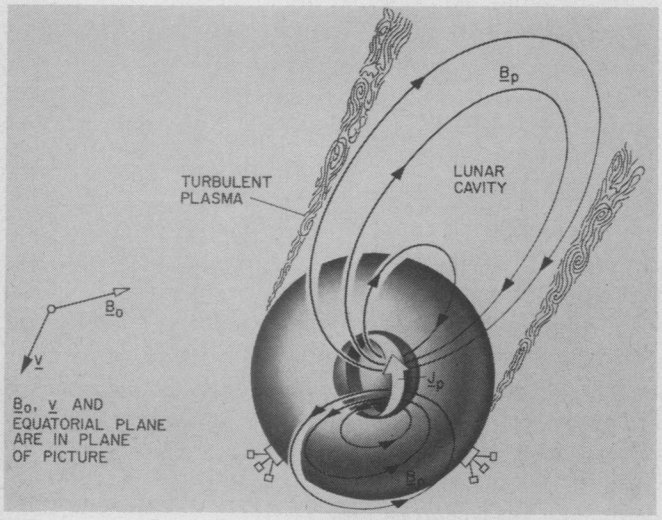

(b)

Fig. 2. Induced lunar magnetic fields. (a) Toroidal field, induced by a $\boldsymbol{V}\times\boldsymbol{B}_0$ driving electric field. The electric field exists due to the motion of a solar magnetic field $\boldsymbol{B}_0$, frozen in the solar wind, past the moon. View shows the side of the moon facing the sun, with lunar north pole at top. (b) Poloidal field, induced by time-dependent fluctuations in the solar magnetic field. View is down upon the lunar northern hemisphere. The lunar equatorial plane, the solar magnetic field $\boldsymbol{B}_0$, and the solar-wind velocity $\boldsymbol{V}$ are in the plane of the paper.

netic field to be uniform over lunar dimensions, and the moon to be homogeneous. Colburn *et al.* also stated that their results were consistent with a model in which the moon has a highly conducting core surrounded by an insulating layer.

In addition to the toroidal lunar field induced by the motional $\boldsymbol{V}\times\boldsymbol{B}$ electric field, there is a poloidal lunar field which is induced by time fluctuations in the solar magnetic field. Eddy currents are induced in the moon by the driving magnetic field; associated with these currents is a poloidal lunar magnetic field which tends to oppose changes in the driving field [see Fig. 2(b)].

Sill and Blank [18] and Schubert and Schwartz [19] have considered the overall time-dependent response of the moon to a time-dependent field. By assuming the proper boundary conditions, it is possible to solve the vector Helmholtz equation for the time-dependent lunar field induced by the time-varying magnetic field and the motional electric field in the solar wind. The magnetometer on Explorer 35 provides a measurement of the external driving field, and the Apollo 12 magnetometer measures the resulting induced lunar fields.

A conductivity σ can be determined as a function of depth in the lunar interior if it is assumed that displacement currents are negligible. After the radial conductivity distribution has been calculated, a material distribution can be assumed, and the internal temperature T can be calculated by using the method of Rikitake [20]; that is,

$$\sigma = \sum_{i=1}^{3} \sigma_i \exp\left[\frac{-E_i}{kT}\right] \tag{2}$$

where E_i is the activation energy of the material, σ_i is the conductivity at infinite temperature, and k is Boltzmann's constant. The three summation terms of (2) denote impurity, intrinsic, and ion semiconduction effects which dominate, respectively, at increasing temperatures. England *et al.* [21] have calculated an internal conductivity distribution based upon thermal models from Phinney and Anderson [22] for a young cold poorly conducting moon and for an old hot highly conducting moon. The hot lunar model has a factor of 10^3 greater interior electrical conductivity than the cold model; therefore, determination of the lunar-interior-temperature profile should allow differentiation between hot and cold models of the moon.

Experimental Method

The magnetometer, designed and built to measure the magnetic fields at the Apollo 12 site, is one of the five instruments of the ALSEP. Astronauts Conrad and Bean deployed the instrument at 1440 hours GMT on November 19, 1969.

The geometric site, instrument sensitivity, and frequency range selected for this magnetometer experiment are based upon the electromagnetic lunar parameters outlined in the previous section. Time variations of the field are required for sounding measurements, and dc fields are required for a measurement of the unipolar interaction and of the permanent lunar magnetic field. Another requirement is that the magnetometer be able to operate during the lunar day and night since the mapping of the field lines to determine the interior configuration requires measurements during a complete lunation. Furthermore, the instrument must provide its own internal calibrations on a periodic basis in order to determine instrument drifts during temperature excursions and over long time periods.

As for earth-based magnetic observatories, it is important that a site survey be conducted at the lunar magnetic observatory location. Local deposits of nickel–iron or stony-iron meteoric material may be magnetized or may produce induction fields which will produce anomalous readings for measurements of the global

TABLE I
APOLLO 12 MAGNETOMETER CHARACTERISTICS

Parameter	Value
Range	0 to ±400 γ 0 to ±200 γ 0 to ±100 γ
Resolution	±0.2 γ
Frequency response	dc to 3 Hz
Angular response	Proportional to cosine of angle between magnetic-field vector and sensor axis.
Sensor geometry	Three orthogonal sensors at the end of 100-cm booms Orientation determination to within 1° in lunar coordinates
Commands	8 ground and 1 spacecraft
Internal calibration and sensor flip	180° flip; 0, ±25, ±50, and ±75 percent of full scale
Field bias offset capability	0, ±25, ±50, and ±75 percent of full scale
Modes of operation	Orthogonal field measurements; gradient measurement; internal calibration
Power	3.5 watts average in daytime 7.5 watts average in nighttime
Weight	8.9 kg
Size	25 by 28 by 63 cm
Operating temperature	−50° to +85° C

field response of the moon. The site survey is accomplished by measuring the vector magnetic field at each of the three sensor heads and calculating the field gradient in the plane of the sensors. This gradient measurement provides information on the location of a point dipole magnetic field source, the minimum scale size of the measured field, and also permits one component of the curl of the total magnetic field to be calculated.

Because the accuracy of an individual measurement will be fixed due to telemetry bit-rate limitations, the instrument must have a variable range, and any set range must be capable of being biased by a known amount. The instrument must also measure its position with respect to the lunar coordinate system. This is accomplished by the use of a gravity level sensor which indicates angles in two orthogonal vertical planes and a shadowgraph reading taken by an astronaut to determine the azimuthal alignment of the magnetometer. The preceding requirements have resulted in the development of an instrument which has the properties listed in Table I and the configuration in Fig. 1.

Fluxgate Sensor

The Ames fluxgate sensor, shown schematically in Fig. 3, is the heart of the magnetometer experiment. Three fluxgate sensors are located at the end of three mutually perpendicular booms (see Fig. 1). Each sensor weighs 25 grams and uses 15 mW of power during operation. It consists of a flattened toroidal core of Permalloy which is driven to saturation by a sine wave at a frequency $f_0 = 6000$ Hz. This constant-voltage sine wave drives the core to saturation during alternate half-cycles and modulates the permeability at twice the drive frequency. The voltage induced on the sense windings is equal to the time rate of change of the net flux contained in the area enclosed by the sense winding. This net flux consists of the flux imparted by the drive winding and the flux imparted by the ambient magnetic field. The drive winding imparts two equal and opposite components of flux at the drive-signal fundamental frequency. In a zero-amplitude magnetic field there is no voltage generated on the sense windings. The presence of an external magnetic field will cause a signal to appear at the sense winding. The signal will be a second harmonic of the drive signal which will be amplitude modulated at a magnitude proportional to the ambient magnetic field. The phase of this second harmonic signal with respect to the drive waveform indicates the polarity of the magnetic field. The sensor electronics amplifies and filters the $2f_0$ sense-winding signal and synchronously demodulates it to derive a voltage proportional to the magnetic field. After demodulation the resulting signal is amplified and fed back to the feedback winding to null out the ambient field. Operating at null increases the thermal stability by making the circuit independent of core permeability variations with temperature.

Electronics Subsystem

The magnetometer electronics is self-contained except for ALSEP-supplied power, telemetry timing, and command lines. It weighs 6 pounds, occupies a volume of 300 cubic inches, and contains 1300 active components, 1800 passive components, and 3300 memory-core locations. The components have been chosen and screened for low magnetic signature and for an operating reliability of 0.99 for one year on the lunar surface.

Fig. 4 is the functional block diagram of the instrument. The operation of the electronics can be categorized as follows:

1) magnetic field measurements
2) housekeeping measurements
3) data processing
4) site survey and calibration sequencing
5) sensor orientation
6) power control
7) thermal control.

The magnetic field measurements are made by the fluxgate sensors, which are operated by the sensor electronics to provide to the analog-to-digital (A/D) converter an open-loop output voltage which is proportional to the field. The gain of the sensor electronics is 2.5×10^3 V/γ. By using 40 γ/volt gain in the feedback loop, a 0- to ±2.5-volt signal is supplied at the output for input fields of ±100 γ. This signal is processed through a low-pass 3-pole Butterworth filter required to reduce aliasing errors at the A/D-converter sample rate of 26.5 samples/s. This filter has 3-dB attenuation at 1.7 Hz and 64-dB attenuation at a sample rate of 26.5 Hz (see Fig. 5). The sensor electronics has three ranges of ±100γ, ±200γ, or ±400γ which can be selected by ground command. Calibration and dc offset fields are generated by producing precisely known currents in the sensor feedback winding. Fig. 6 shows data taken during the self-calibration mode.

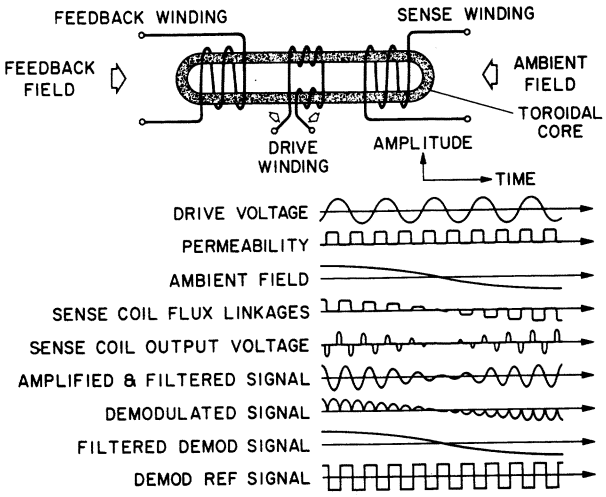

Fig. 3. Schematic outline of the Ames fluxgate sensor.

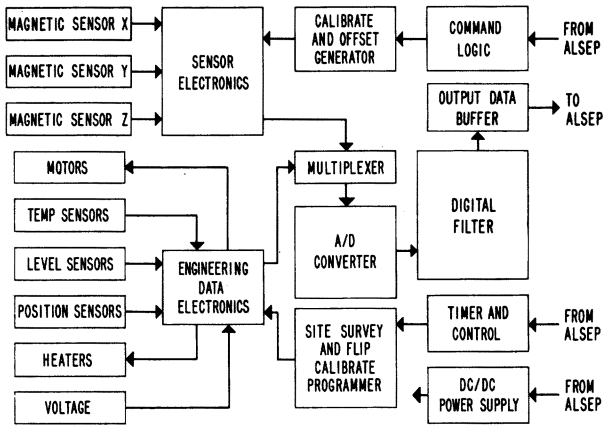

Fig. 4. Functional block diagram for the lunar surface magnetometer electronics.

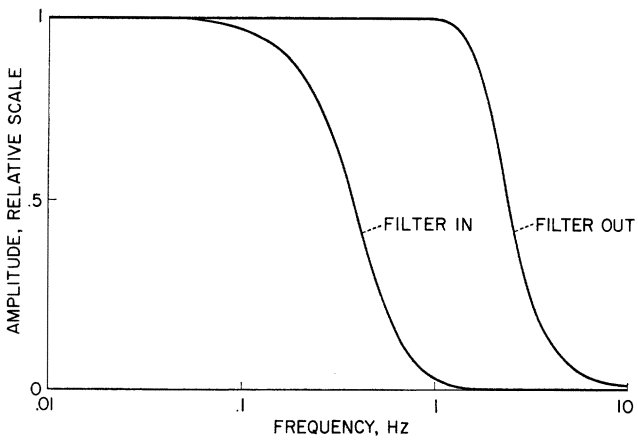

Fig. 5. Frequency response of the lunar surface magnetometer electronics, as measured through the telemetry link, with the digital filter in the circuit and with the digital filter bypassed.

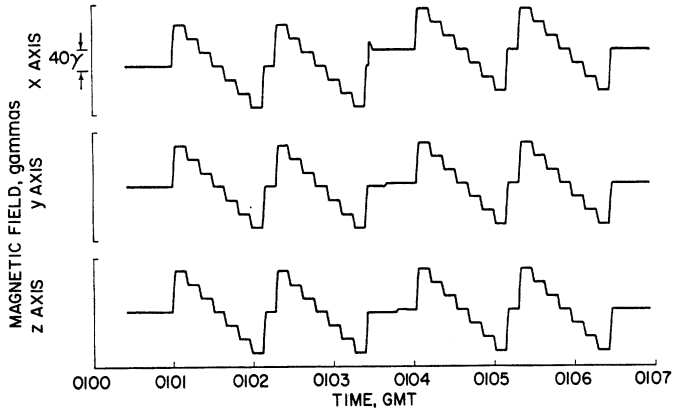

Fig. 6. The magnetometer in self-calibration mode, which involves internal insertion of biases of 75, 50, 25, 0, −25, −50, and −75 percent of instrument full scale. This bias sequence is performed twice; then all three sensors are flipped 180°, and the bias sequence is repeated two more times.

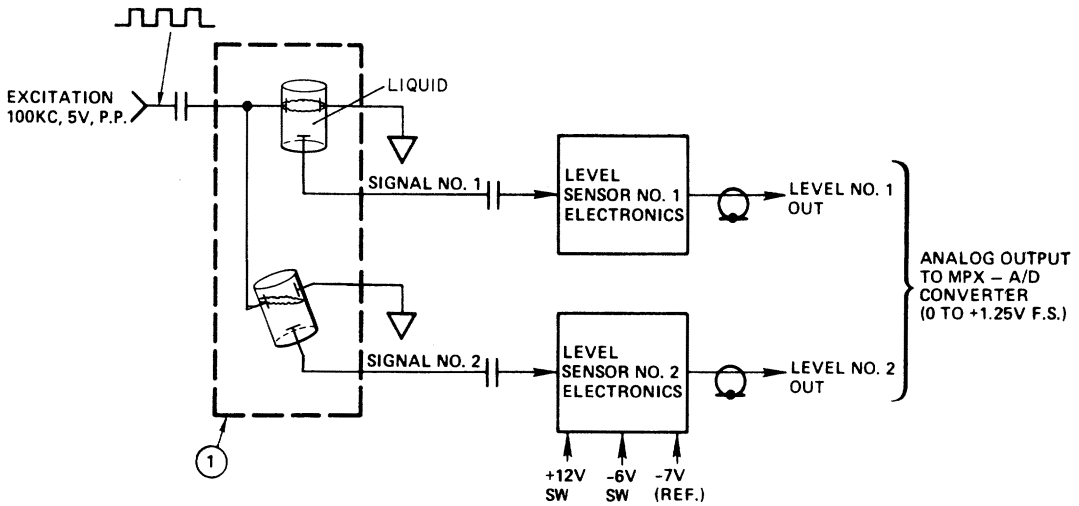

Fig. 7. Gravity level sensor electronics.

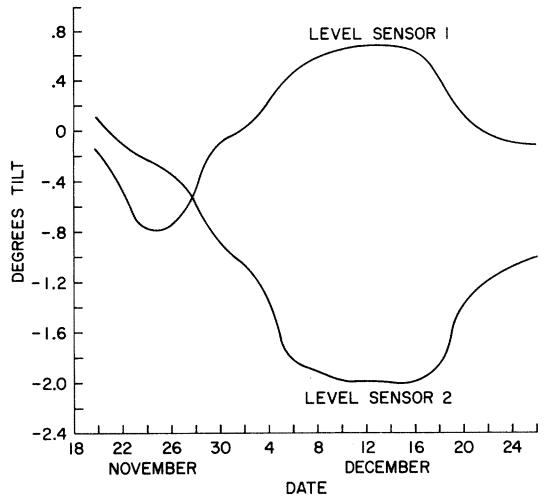

Fig. 8. Level sensor data for the first postdeployment lunation. The magnetometer site was in darkness during the period December 4–18, 1969, and in sunlight the rest of the time shown.

Two orthogonal gravity level sensors are used to measure the tilt angle of the magnetometer on the lunar surface. These sensors supply a 0 to ± 1.25-volt signal to the A/D converter for angles of tilt between -15 to $+15°$. The sensors use an electrolytic fluid sensing element with electrodes located in positions shown in Fig. 7. The tilt angles are transmitted back to earth once every 5 seconds to 0.2° accuracy. Level-sensor data curves for the first lunation are shown in Fig. 8.

The housekeeping measurements are made by the engineering-data-electronics subsystem. Five temperatures are measured with thermistor-resistor networks shown in Fig. 9 at various locations in the magnetometer, and an analog signal of 0 to $+1.25$ volts is supplied to the A/D converter for temperatures from -50 to $+125°C$. The temperature of the fluxgate sensors is actively controlled by one of the thermistors to within $\pm 3°C$ by resistance heaters driven by the engineering data electronics.

Three motors are used to flip and gimbal the fluxgate sensors during lunar operations. The motors are driven by the engineering data electronics upon ground command or internally generated ALSEP commands. The sensor orientation is measured by position sensor capacitors at 0, 90, and 180° and by a microswitch for the gimbal positions of 0 and 90°. The output of these position sensors is encoded into a two-bit status word and transmitted to the output data buffer.

A 5.0-volt reference signal is stepped down to 1.0 volt and transmitted to the A/D converter for monitoring. This reference voltage is used throughout the instrument for calibration, level sensing, etc.

Internal data processing of the magnetic field measurements requires the major portion of the magnetometer electronics. The analog data is converted to digital form by the A/D converter and then filtered by the digital filter and transferred to the output data buffer. There are two important reasons that the magnetometer must provide internal data processing. One reason is to provide the maximum amount of data for the available telemetry bit rate for a system which is not read out continuously. The second reason is that in order to introduce minimum error into the data by the sampling process, the data must be sampled in a synchronous manner and frequency limited by a filter. The reason for frequency limiting is the Nyquist sampling theorem which states that in order for a frequency-limited signal to be sampled by a perfect switch without error, the sampling rate must be at least twice the highest frequency of the signal. In actual practice, the filter cutoff frequency which limits the signal spectrum is not an ideal function, nor is the switch perfect. For these reasons, the cutoff frequency is generally limited to much less than one-half the sampling frequency.

The magnetometer has two samplers: the A/D converter and the ALSEP data sampler. In order to minimize aliasing errors the prealias filter in the sensor electronics has a 3-dB point at 1.7 Hz for an ALSEP sampling rate of 3.3 Hz. Using these filtering constants, a 4-pole Bessel digital filter was designed and built to limit the alias error to less than 0.05 percent and to have less than 1 percent overshoot for a step-function response. This filter has a bandwidth of 0 to 0.36 Hz and will permit magnetic field measurements to be made over an entire lunar cycle, allowing less than 0.1 percent alias errors to be incorporated into the data for input signals with constant-amplitude frequency content. The filter is a hard-wired digital computer which accepts the 10-bit word from the A/D converter, stores it in a 3300-bit-core-storage memory unit, performs the arithmetic operations for the filter routine, and transfers the data to the output data buffer. It can be bypassed by ground command in order to pass higher frequency information. Frequency response for the entire system is shown in Fig. 5.

The dc/dc converter is designed to provide regulated $+15$, $+7$, $+6$, -7, and -15 volts dc to the magnetometer electronics for ALSEP power-line excursions from 24 to 30 volts dc. Power switching is used throughout the instrument in order to minimize power consumption. The average power used by the magnetometer is 3.5 watts, with switching variations from 1.8 to 10 watts.

Mechanical Subsystem

The main function of the mechanical subsystem on the magnetometer is to orient the fluxgate sensors in three mutually orthogonal directions and to reorient these sensors automatically for calibration and site-survey operations. The sensors are spread approximately 150 cm apart and are kept 70 cm above the lunar surface. A deployed instrument is shown in Fig. 1. A functional schematic of the motor and cables necessary to flip and gimbal the fluxgate sensor is shown in Fig. 10. The toggle is used to produce a bistable mechanical system which holds the fluxgate sensor in a preferred scientific orientation in case of a mechanical malfunction.

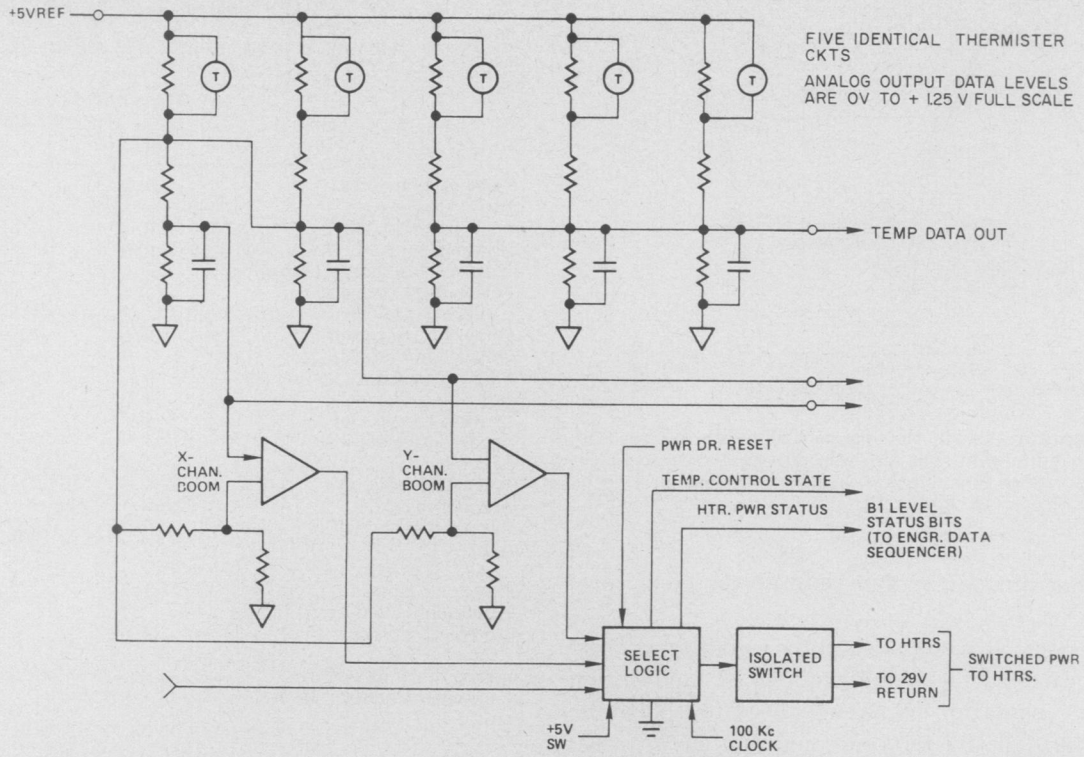

Fig. 9. Temperature-monitor electronics.

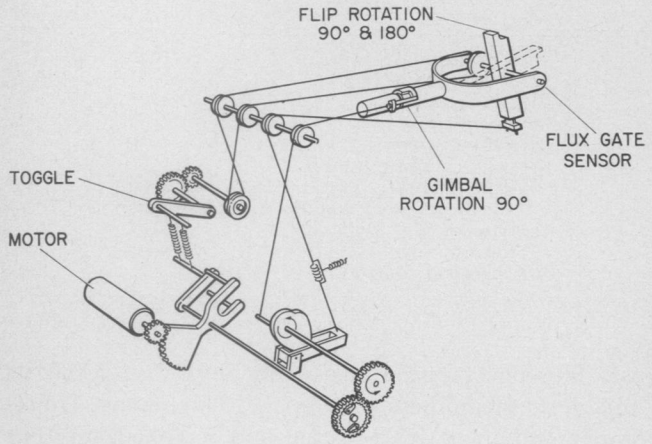

Fig. 10. Mechanical gimbal and sensor-flip unit.

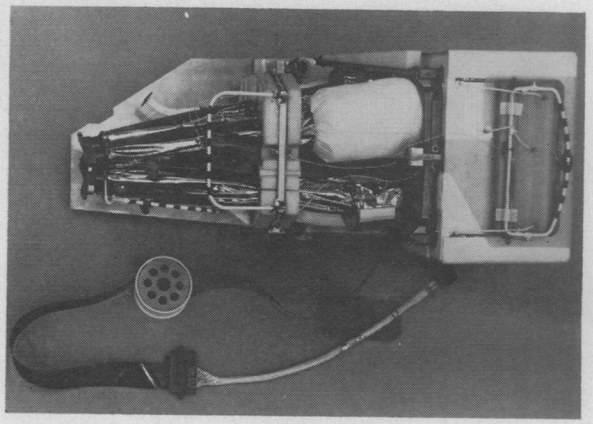

Fig. 11. The lunar surface magnetometer in stowed configuration.

During a site-survey mode of operation the sensors are flipped and rotated in order to measure simultaneously at all three sensors each of three orthogonal components of the magnetic field. This allows calculation of the gradient in the plane of the sensors. The orientation accuracy is better than ± 1.5 percent for all modes of operation.

Another very important feature of the mechanical subsystem is the capability to fold the extended booms for stowage during transit to the moon (see Fig. 11). The instrument is also designed so that the astronaut is able to unfold the sensor booms and legs, level and align the instrument, and read the azimuthal angle back to earth over the voice communication system. Environmental constraints required the instrument to be vibrated sinusoidally from 10 to 50 Hz at 13 times the acceleration due to gravity (13*g*), 50 to 100 Hz at 26*g* and 100 to 200 Hz at 20*g*. Thermal vacuum constraints required that the mechanical subsystem operate in the internal temperature range of -30 to $+65$°C and to continue to operate after reaching the temperature extremes of -50 and $+85$°C.

Thermal Subsystem

The thermal subsystem on the magnetometer is designed to keep the magnetometer between -30 and $+65$°C during the night and day excursions. Lunar dust on the thermal control surfaces of the Apollo 12 magnetometer, however, is expected to have caused the instrument electronics of that particular instrument to

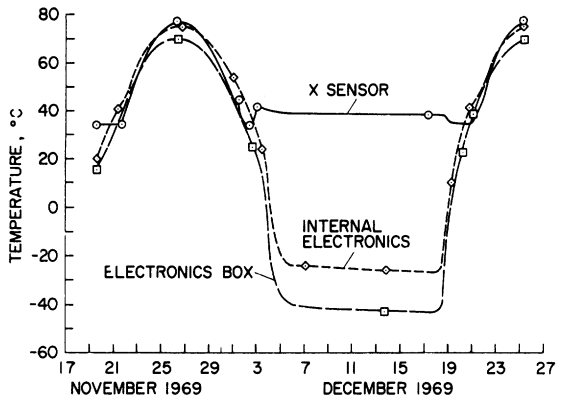

Fig. 12. Temperatures inside the magnetometer during the first postdeployment lunation. The sun was directly overhead at the magnetometer site on November 26; sunset occurred on December 4, and sunrise on December 18.

rise 10°C higher during the day than predicted by prelaunch tests.

Thermal control is accomplished by a combination of insulation, control surfaces, and heaters. A covering of highly efficient insulation blankets is used to isolate the instrument thermally from its surroundings so that a set of parabolic reflector arrays (as shown in Fig. 1) can control the heat transfer between the instrument and the lunar environment. The 1/2-inch-thick insulation blanket is composed of 40 layers of 1/4-mil aluminized mylar separated by 40 layers of 3-mil-thick glass fiber. The parabolic reflector array consists of a vertical low-emittance reflector located above a horizontal high-emittance radiating fin. Thermal radiation emanating from the lunar surface is reflected away by the parabolic array while internally generated heat is dissipated to space. The area of the parabolic reflector array is adjusted to provide the proper thermal resistance to maintain the instrument within its operating temperature limits. The instrument is aligned to within $\pm 5°$ of the solar ecliptic plane so that solar radiation does not impinge directly on the radiator fins of the reflector array.

Electric heaters are installed in the fluxgate sensor housings and in the electronics box in order to compensate for various heat leaks in the system. There are four separate thermal subsystems: the electronics box and each of the three sensor heads. An adiabatic point exists on each boom approximately halfway between the sensor and the electronics box. Each sensor head contains a thermal control surface, glass heat felt insulation, and resistance heaters which are servo controlled by thermistors on the fluxgate sensors. Fig. 12 shows the temperature measured inside the electronics, outside the electronics case, and in the X fluxgate sensor head. The duty cycle for the 1-watt heaters in each head and the 2.8-watt heaters in the box was 0 percent during the day and 85 percent during the lunar night.

The most severe constraint placed on this experiment was to keep the magnetic field below 2γ at a radius of 3 feet from the instrument centroid after exposure to 25 gauss. This necessitated advancing the state of the art in magnetic cleanliness of a space instrument. Unless each part was properly selected and screened, any one of the 3000 piece parts that make up the electronics could exceed the 2γ at 3 feet. All interconnect modules were constructed as shown in Fig. 13 so that all ground return currents would cancel out fields produced by input currents into the module. As seen in Table II the field from the instrument is on the order of 3.0γ at 3 feet after a 25-gauss perm. After deperm the field goes well below the 0.2γ maximum sensitivity of the instrument.

TABLE II
LUNAR SURFACE MAGNETOMETER MAGNETIC PROPERTIES

	Measured 12-Inch Test Radius Permed: 25 Gauss		
	$X(\gamma)$	$Y(\gamma)$	$Z(\gamma)$
Sensor electronics	5.4	9.5	5.5
Input driver	0.3	1.2	0.2
Sensor driver	0.7	0.3	0.5
Power filter	0.4	.6	0.55
Engineering data electronics	14.0	14.7	9.7
MPX-A/D converter	5.4	2.0	5.2
Calibration offset bias generator	11.1	4.2	2.4
Output data buffer	0.8	0.0	2.65
Offset command logic	1.0	0.0	3.0
Engineering data sequencer	0.6	0.05	1.65
Arithmetic unit	4.0	0.2	17.5
System timer	4.25	2.9	4.3
dc/dc converter	3.0	6.4	3.0
Memory	13.3	16.9	16.8
Scientific sequencer	4.8	0.15	8.35
Site survey	1.3	0	4.4
Electromechanical site survey	10.0	5.9	1.1
Total	80.4	66.0	86.8
Permed: 25 gauss Equivalent field at 36 inches (total ÷ 27)	3.0	2.4	3.2
Depermed: 50 gauss Equivalent field at 36 inches (total ÷ 27)	<0.1	<0.1	<0.1

TABLE III
COMMAND LIST

1) Operational power ON
2) Power standby
3) Range select
4) Field offset
5) Offset address
6) Flip-calibrate inhibit
7) Flip-calibrate initiate (also initiated every 12 hours by the ALSEP timer)
8) Digital filter bypass
9) Site survey
10) Thermal control

Date Telemetry

The Apollo 12 magnetometer experiment is controlled from the Manned Spacecraft Center (MSC), Houston, Tex., by commands transmitted to ALSEP from remote tracking stations. These commands are chosen on the basis of the analysis of data received in real time at MSC and are transmitted to the ALSEP by the manned space flight network (MSFN). Fig. 14 shows a simplified block

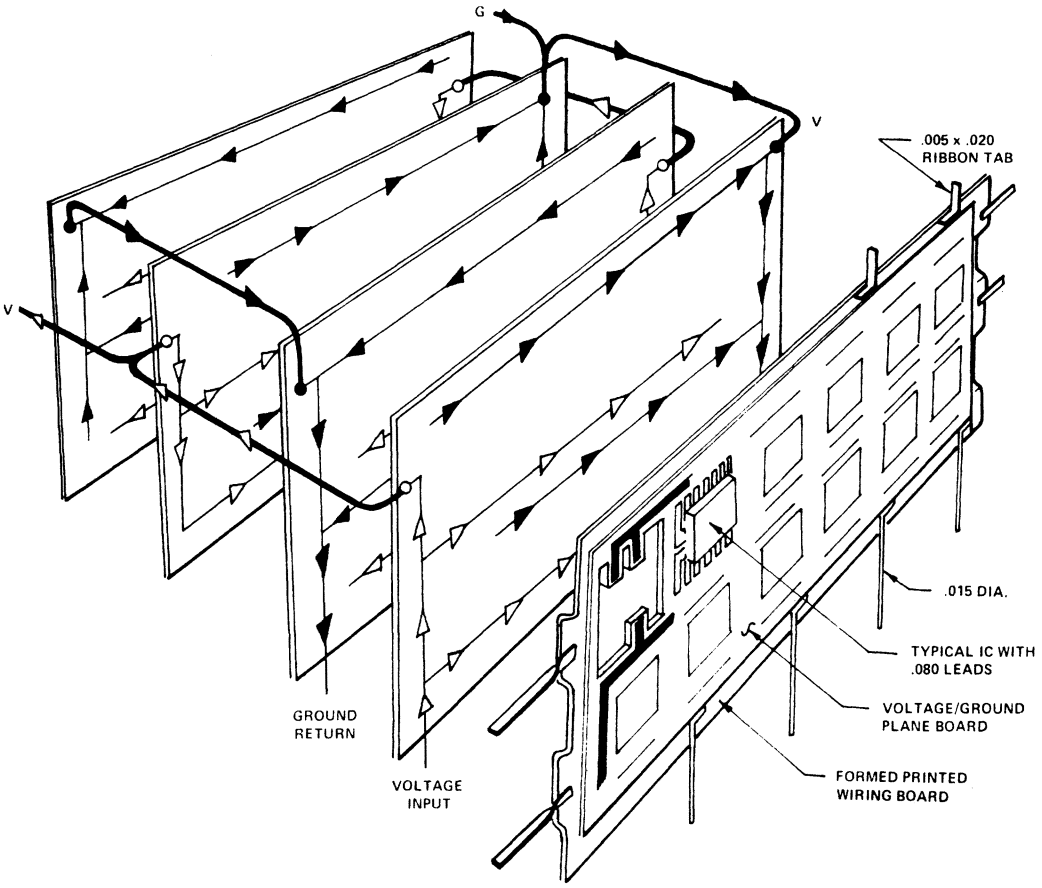

Fig. 13. Ground and voltage line layout for an interconnect module showing the wiring scheme used to minimize net magnetic fields due to current flow in the module. Arrows indicate current flow.

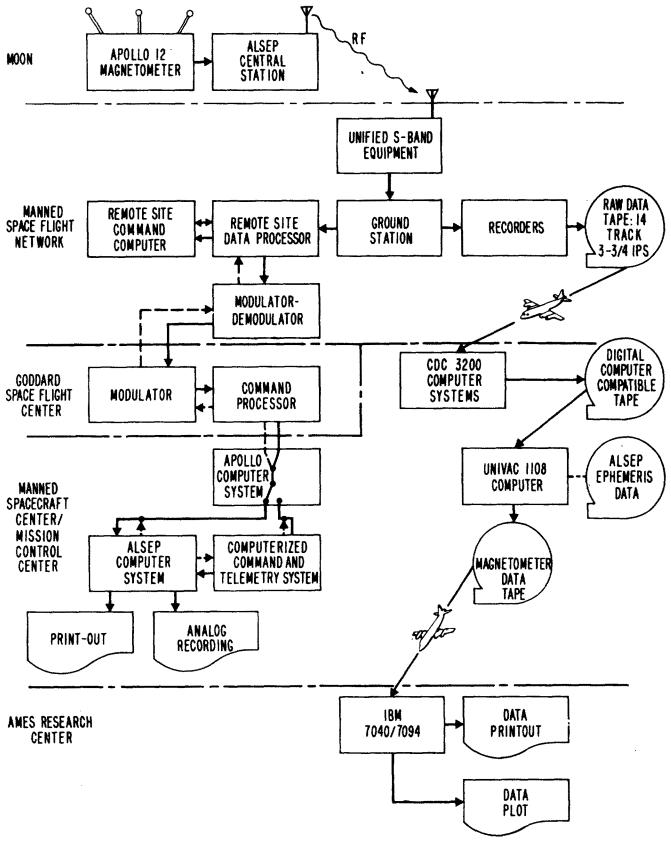

Fig. 14. Outline of telemetry command and data flow from the magnetometer to Ames Research Center.

diagram of the telemetry command and data flow. There are ten ground commands and one ALSEP-timer-initiated command which control the magnetometer. Table III lists these commands.

Science and engineering data are continuously transmitted back to earth from the magnetometer experiment. Each analog sensor output is converted to a digital word and transmitted to earth via the telemetry format shown in Table IV. The digital data is recorded on magnetic tape at the remote sites and sent to MSC for processing. These processed tapes are then sent to Ames Research Center for detailed scientific postmission analysis.

In addition to being recorded on magnetic tape for later use, the data are sent directly to MSC for real-time analysis in order to allow proper control of the experiment. Real-time control is necessary in order to establish the proper range, offset, frequency response, thermal control, etc. One of the most important requirements for real-time operation is to control the one time-irreversible sequence of events which performs the gradient measurements during a site survey. It is necessary to assess both the magnetic-field amplitude stability and the instrument performance before sending the command to start the site-survey internal sequences. Data for the real-time operations are presented continuously on a chart recorder and intermittently on a high-speed printer upon command.

TABLE IV
TELEMETRY DATA

ALSEP Word	Subcommutated Channel (bit 10)	Engineering Analog, 7 Bit (bits 3 to 9)	Status Bits 1	Status Bits 2
5	1	X-sensor temperature	X-flip position	X flip
	2	Y-sensor temperature	Y flip	Y flip
	3	Z-sensor temperature	Z flip	Z flip
	4	gimbal flip unit temperature	X gimbal	Y gimbal
	5	electronics temperature	Z gimbal	temperature control
	6	level detector 1	spare	heater state
	7	level detector 2	range	range
	8	reference voltage	spare	spare
	9	same as 1	X offset	X offset
	10	same as 2	X offset	Y offset
	11	same as 3	Y offset	Y offset
	12	same as 4	Z offset	Z offset
	13	same as 5	Z offset	Z offset
	14	same as 6	address	address
	15	same as 7	filter	inhibit
	16	same as 8	spare	spare
ALSEP Word	Polarity Bit (bit 10)	Field Component Amplitude (bits 1 to 9)		
17	10	X-axis magnetic field		
19	10	Y-axis magnetic field		
21	10	Z-axis magnetic field		
49	10	X-axis magnetic field		
51	10	Y-axis magnetic field		
53	10	Z-axis magnetic field		

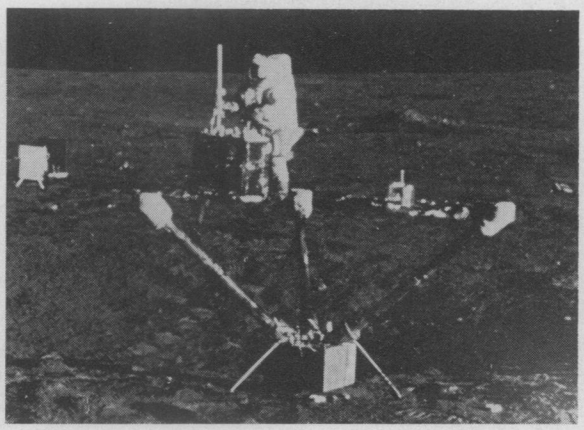

Fig. 15. The Apollo 12 lunar surface magnetometer deployed on the moon in the Ocean of Storms. The Z sensor is at right, directed east, while the X and Y sensors are at middle and left, respectively. In the background, Astronaut Conrad is shown adjusting the S-band antenna on the central station.

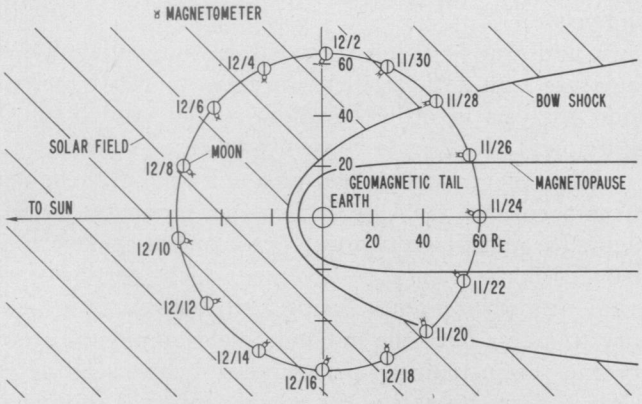

Fig. 16. Lunar orbit during the first postdeployment lunation, 1969. During a complete revolution about the earth, the magnetometer passes through the earth's bow shock, the magnetosheath, the geomagnetic tail, and the interplanetary region dominated by solar-plasma fields.

TABLE V
APOLLO 12 MAGNETOMETER EXPERIMENT OPERATIONS

Date	Time (GMT)	Operation
November 14, 1969	1622	lift-off from Kennedy Space Center
November 18, 1969	1432	lunar landing
November 19, 1969	1255	ALSEP removed from lunar module
November 19, 1969	1341	magnetometer removed from ALSEP
November 19, 1969	1401	magnetometer deployed by Conrad and Bean
November 19, 1969	1402	magnetometer photographed
November 19, 1969	1439	magnetometer turned ON
November 19, 1969	1445	magnetometer range selected
November 20, 1969	1109	first flip-calibrate sequence completed
November 20, 1969	1426	lunar module ascent
November 22, 1969	2250	site-survey sequence started

RESULTS

The Apollo 12 mission provided the first magnetic-field measurements from the lunar surface. The magnetometer was placed on the lunar surface at the position 23.35° west longitude and 2.97° south latitude in selenographic coordinates. The sequence of operations during the first part of the mission is given in Table V.

The experiment is deployed so that each sensor is directed approximately 35° above the horizontal. The Z sensor is pointed toward the east and the X sensor roughly toward the northwest. The Y sensor completes a right-handed orthogonal system. A photograph of the deployed instrument taken by Astronaut Bean is shown in Fig. 15. This photograph was taken after Bean had leveled and azimuthally aligned the instrument along the ALSEP-to-sun line by moving the instrument around until the bubble level and shadowgraph read within marked preset values. The shadowgraph reading was transmitted over the voice telemetry link and indi-

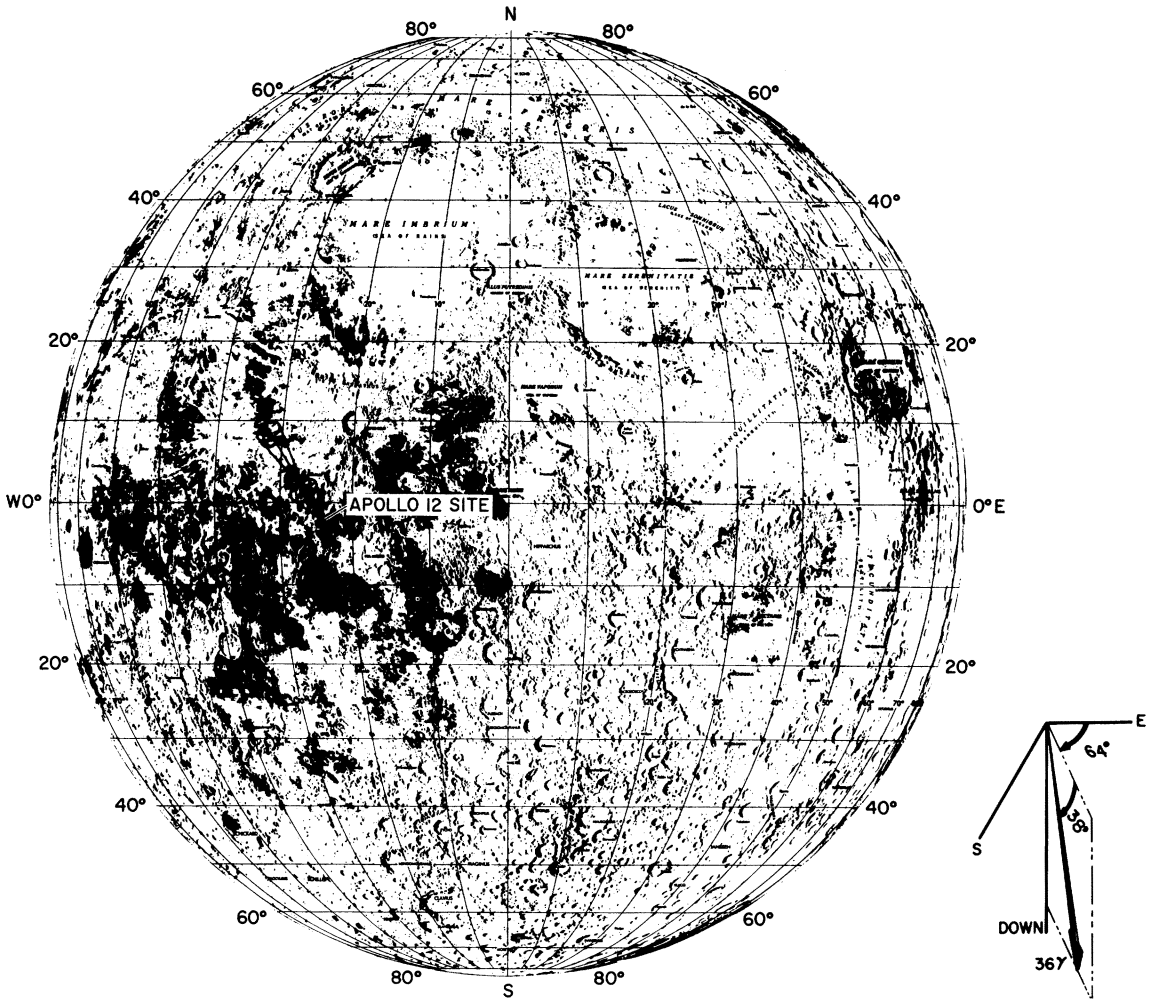

Fig. 17. Apollo 12 magnetometer site on the moon (23.35° west longitude, 2.97° south latitude). The arrow shows the approximate orientation of the measure 36γ steady field, while the insert shows the steady field directed downward into the lunar surface at an elevation angle 38° from the horizontal and an azimuth angle 64° clockwise from due east.

cated that the instrument was aligned azimuthally to within 0.5° of the instrument shadowgraph-to-sun line. The orthogonal electronic level sensors are monitored every 5 seconds as part of the magnetometer engineering data. The angular readings are shown in Fig. 8 and indicate that the instrument changed its orientation by about 2° during the first lunar day–night period.

During each orbit around the earth, the moon is embedded in each of the different magnetic-field regions shown schematically in Fig. 16. The magnetic-field environment is dominated by the solar wind in interplanetary space, by the interaction of the solar wind and the earth magnetic field in the bow shock and magnetosheath region, and by the earth's intrinsic field in the geomagnetic tail. A detailed measurement of the magnetic field as a function of time on the lunar surface in the immediate vicinity of the moon will permit the electrical conductivity σ, permeability μ, and dielectric constant ϵ to be calculated. These electrical parameters that are calculated for field measurements at one point on the lunar surface may be associated with either the whole moon or with that part of the lunar body in the vicinity of the Apollo 12 landing site. A magnetometer network is required in order to measure unambiguously the whole-body inductive response of the moon to time-varying magnetic fields.

Magnetic-field data were received immediately after instrument turn-on, and ground commands were sent to establish the proper range, field offset, and operational mode for the instrument. Low-frequency magnetic-field data have been averaged over the first 20-day period. A preliminary examination indicates that the average field magnitude is $36 \pm 5\gamma$ and that the field is directed downward, 38° from the horizontal and 64° south of east, as shown in Fig. 17. A more detailed analysis over a period of several lunations will be required in order to reduce the uncertainty in this measurement.

A site survey was performed during a 2-hour period starting at 2250 hours GMT on November 22, 1969. The magnitudes for the vector measurements at each of the sensor-head locations are as follows.

Sensor	Magnetic-Field Magnitude
X	$32.7 \pm 0.2\gamma$
Y	$32.7 \pm 0.2\gamma$
Z	$32.8 \pm 0.2\gamma$

The field gradient in a plane parallel to the lunar surface is less than the instrument resolution of 4×10^{-3} γ/cm. The indication of a very low gradient and the absence of an observed field change during lunar module ascent demonstrate that the field source cannot be a magnetized artifact. Internal instrument calibrations have been initiated by ground commands which have rotated the sensors, cycled through the zero offsets, and operated the gradiometer sequence. In addition, ground commands have been used to change ranges from $\pm100\gamma$ to $\pm200\gamma$ and $\pm400\gamma$ in order to measure the steady field repeatedly in different instrument operation modes.

If this measured 36γ field were due to a dipole source located at the center of the moon, it would imply that the global magnetic moment is $M\sim1.7\times10^{21}$G·cm^3. Magnetometers on the lunar-orbiting Explorer 35 satellite [2], [3], [7] showed that a centered lunar dipole moment would have strength less than the order of 10^{20}G·cm^3 based upon the absence of any measurable field attributable to the moon at the altitude of the satellite. It follows, therefore, that the measured 36γ field is due to a localized source near the Apollo 12 site. The surface Apollo 12 field intensity and gradient upper limit together with recent Explorer 35 data permit the equivalent source to be located a distance 0.2 km$\lesssim R\lesssim$200 km from the magnetometer and to have a magnetic moment in the range $1.4\times10^{9}<M<1\times10^{18}$G·cm^3. The areal location and magnetic-moment bounds indicated by the magnetic field measurements imply an extended source with remanent magnetic properties similar to those found in the Apollo 11 samples [23]. The high coercivities and Curie temperatures of the Apollo 11 samples imply that native iron is the dominant magnetic constituent of the samples [23].

The time-dependent response of the moon to fields in the magnetosheath is shown in Fig. 18. This is a time-series plot of Apollo 12 magnetometer data correlated with Explorer 35 data which has been transformed into the same coordinate systems. Explorer 35 has a periselene of 2570 km and an aposelene of 9380 km. As shown in Fig. 18, the horizontal (Y and Z) components of the magnetic field at the Apollo 12 site are amplified when compared to the Explorer 35 measurements. Detailed analysis of this inductive response to the solar-wind plasma should permit the electrical conductivity of the lunar interior to be calculated.

In summary, a magnetometer experiment has been designed, fabricated, tested, and deployed on the lunar surface. The instrument has measured the surface magnetic field while the moon has passed through the earth's magnetic bow shock, the magnetosheath, the geomagnetic tail, and in the solar wind during both lunar daytime and nighttime. These data are presently being reduced and analyzed in order to determine lunar electromagnetic properties and to place bounds on the interior temperature and composition of the moon.

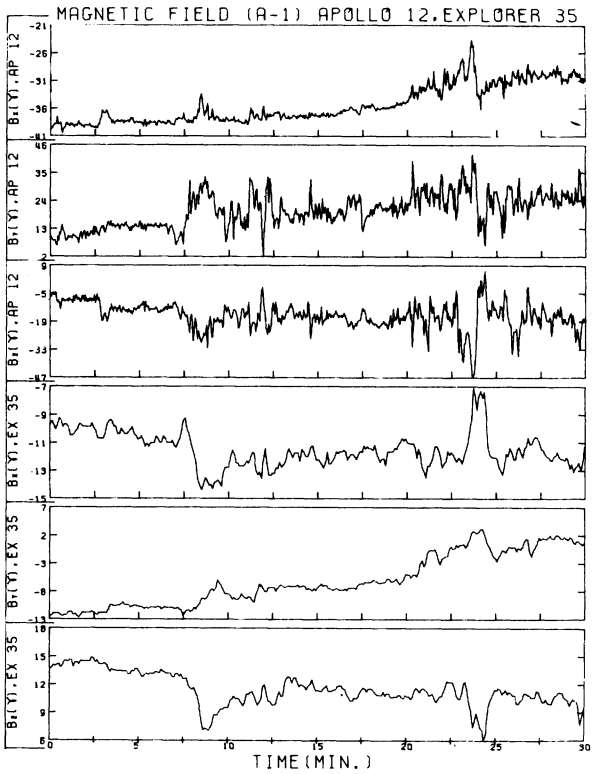

Fig. 18. Simultaneous time-series magnetic-field data from the Apollo 12 magnetometer and the lunar-orbiting Explorer 35 satellite while the moon is located inside the earth's magnetosheath. Data are plotted in a lunar surface coordinate system which is oriented with x toward the zenith, y east, and z north.

Acknowledgment

The authors wish to thank the ALSEP project office at the Manned Spacecraft Center, Houston, Tex., for making this experiment possible; the Philco-Ford Corporation, Palo Alto, Calif., for translating our functional specifications into hardware; and the staff at the Ames Research Center for all their support in this experiment.

References

[1] Sh. Sh. Dolginov, E. G. Eroshenko, L. N. Zhuzgov, and N. V. Pushkov, "Measurements of the magnetic field in the vicinity of the moon by the artificial satellite Luna 10," *Doklady, Akad. Nauk USSR*, vol. 170, pp. 574–577, September 21, 1966.

[2] C. P. Sonett, D. S. Colburn, and R. G. Currie, "The intrinsic magnetic field of the moon," *J. Geophys. Res.*, vol. 72, pp. 5503–5507, November 1, 1967.

[3] N. F. Ness, K. W. Behannon, C. S. Scearce, and S. C. Cantarano, "Early results from the magnetic field experiment on lunar Explorer 35," *J. Geophys. Res.*, vol. 72, pp. 5769–5778, December 1, 1967.

[4] ——, "Apollo 11 preliminary science report," NASA, SP-214, 1969.

[5] J. N. deWys, "Results and implications of magnet experiments on Surveyor 5, 6, and 7 spacecrafts," *Trans. Amer. Geophys. Union* (Abstracts), vol 49, p. 249, March 1968.

[6] G. V. Keller and F. C. Frischknecht, *Electrical Methods in Geophysical Prospecting*. New York: Pergamon, 1966, p. 58.

[7] K. W. Behannon, "Intrinsic magnetic properties of the lunar body," *J. Geophys. Res.*, vol. 73, pp. 7257–7268, December 1, 1968.

[8] T. Hagfors, "Review of radar observations of the moon," *The Nature of the Lunar Surface*, W. N. Hess, D. H. Menzel, and J. A. O'Keefe, Eds. Baltimore, Md.: The Johns Hopkins Press, 1966, pp. 229–239.

[9] W. E. Brown, Jr., G. B. Gibson, D. O. Muhleman, *et al.*, "Surveyor III mission report—Pt. II. Scientific results," Jet

Propulsion Laboratory, Pasadena, Calif., Tech. Rep., TR 32-1177, ch. 6, pp. 189–194, June 1, 1967.
[10] Z. Kopal, *An Introduction to the Study of the Moon*. The Netherlands: D. Reidel, 1966, p. 369.
[11] D. W. Strangway, "Moon: electrical properties of the uppermost layers," *Science*, vol. 165, pp. 1012–1013, September 5, 1969.
[12] D. S. Colburn, R. G. Currie, J. D. Mihalov, and C. P. Sonett, "Diamagnetic solar-wind cavity discovered behind moon," *Science*, vol. 158, pp. 1040–1042, November 24, 1967.
[13] P. J. Coleman, Jr., "Turbulence, viscosity, and dissipation in the solar-wind plasma," *Astrophys. J.*, vol. 153, pp. 371–388, 1968.
[14] K. L. McDonald, "Penetration of the geomagnetic secular field through a mantle with variable conductivity," *J. Geophys. Res.*, vol. 62, pp. 117–141, March 1957.
[15] T. Gold, "The magnetosphere of the moon," in *The Solar Wind*, R. J. Mackin, Jr., and M. Neugebauer, Eds. New York: Pergamon, 1966, pp. 381–389.
[16] C. P. Sonett, "Principle of planetary unipolar generators," *Planetary Electrodynamics*, vol. 2, S. C. Coroniti and J. Hughes, Eds. New York: Gordon and Breach, 1969.
[17] N. F. Ness, "Electrical conductivity of the moon," *Trans. Amer. Geophys. Union* (Abstracts), vol. 49, p. 242, March 1968.
[18] W. R. Sill and J. L. Blank, "Methods for estimating the electrical conductivity of the lunar interior," *J. Geophys. Res.*, vol. 75, pp. 201–210, January 1, 1970.
[19] G. Schubert and K. Schwartz, "A theory for the interpretation of lunar surface magnetometer data," *The Moon*, vol. 1, pp. 106–117, 1969.
[20] T. Rikitake, *Electromagnetism and Earth's Interior*. Amsterdam, The Netherlands: Elsevier, 1966.
[21] A. W. England, G. Simmons, and D. Strangway, "Electrical conductivity of the moon," *J. Geophys. Res.*, vol. 73, pp. 3219–3226, May 15, 1968.
[22] R. A. Phinney and D. L. Anderson, "Internal temperatures of the moon," Dept. of Elec. Eng., University of Minnesota, Minneapolis, Tycho Study Group Rep., August 1965.
[23] S. K. Runcorn, D. W. Collinson, W. O'Reilly, A. Stephenson, N. N. Greenwood, and M. H. Battey, "Magnetic properties of lunar samples," *Science*, vol. 167, pp. 697–699, January 30, 1970.

An Overview of the Orbiting Astronomical Observatory

JACK SARGENT

***Abstract*—The world's first Orbiting Astronomical Observatory, OAO-II, was launched by the U.S.A. on December 7, 1968. Over one year of operation has proven its design concepts and utility.**

Built in an octahedron shape, 10 feet by 7 feet, the satellite weighs 4400 pounds. Two experiments are located centrally within the spacecraft, each viewing space from opposite ends. Both experiments contain multiple optical and detector systems for spectrophotometry and surveys in the ultraviolet spectrum.

The design was dictated by the stringent requirements of the experiments for pointing accuracy (one minute of arc anywhere in the celestial sphere), pointing stability (five seconds of arc), command capability, data handling, thermal environment, and the constraints of the orbit for ground-station contacts.

Six two-gimbal star trackers are programmed by the on-board memory to acquire and track appropriate guide stars. Error signals are generated which drive the reaction wheels to obtain stellar stabilization. Coarse momentum wheels are used for slewing the spacecraft.

Memories permit storage of 200 000 bits of experimental data. All information is relayed to the central control station in Greenbelt, Md.

OAO-II has shown that it is practical to maintain a continuous viewing capability in space for long periods of time so that fruitful astronomical experiments can be performed.

Manuscript received May 8, 1970. This paper was presented at the 1970 IEEE International Geoscience Electronics Symposium, Washington, D. C., April 14–17.

The author is with NASA, Goddard Flight Center, Greenbelt, Md. 20770.

Introduction

ASTRONOMY is one of the oldest branches of science in existence today. As in other fields of science its study on the more sophisticated level depends on measuring, interpreting, and understanding the nature of the oscillating phenomena that exist on both the micro and macroscopic levels. In our particular case we are concerned with investigating that portion of the electromagnetic spectrum which cannot be viewed from earth due to atmospheric absorption, that is, the ultraviolet region in the range of 1000–4000 Å.

Our job, from an engineering standpoint, was to design, build, test, and launch a satellite containing ultraviolet optical telescopes which could be pointed anywhere in the celestial sphere to an accuracy of one minute of arc and have a stability of 5 seconds of arc. OAO-II was launched in December, 1968, and has now successfully completed 16 months of operation. During this time some 3300 observations have been made with the University of Wisconsin spectrometers and 8200 ultraviolet pictures (2° by 2°) have been recorded by the Smithsonian ultraviolet vidicons.

Launched by an Atlas-Centaur from Cape Kennedy, the spacecraft circles the earth at an altitude of 480 mi,